Earth Syst. Sci. Data Discuss., https://doi.org/10.5194/essd-2018-62
Manuscript under review for journal Earth Syst. Sci. Data
Discussion started: 4 June 2018

Open Access Earth System Science Data Discussions

Spatial and seasonal patterns of near-surface humidity in the foothills of the Canadian Rocky Mountains, 2005-2010

Wendy H. Wood[1], Shawn J. Marshall[1], and Shannon E. Fargey[2]

[1]Department of Geography, University of Calgary, Calgary AB, T2N 1N4, Canada
[2]Department of Geography, University of Victoria, Victoria BC, Canada

Correspondence to: Shawn Marshall (shawn.marshall@ucalgary.ca)

Abstract. Near-surface humidity was monitored from 2005 to 2010 in a mesoscale network of 232 sites in the foothills of the Rocky Mountains in southwestern Alberta, Canada. The monitoring network covers a range of elevations from 890 to 2880 m above sea level and an area of about 18,000 km2, sampling a variety of topographic settings and surface environments with an average spatial density of one station per 78 km2. Hourly screen-level temperature and relative humidity were recorded over the study period, forming the basis for daily mean relative humidity and vapour pressure estimates. Hourly air pressure measurements at Calgary Airport are adjusted for elevation to calculate specific humidity from the vapour pressure. Daily mean specific humidity, relative humidity, and vapour pressure from the multi-year study are available at https://doi.pangaea.de/10.1594/PANGAEA.889435. This manuscript describes the processing methods used to quality-control and gap-fill the data. Overall data coverage for the study period is 89%. Inverse-distance weighting techniques are used to estimate the missing 11% of data, based on neighourhood values of daily mean specific humidity. We report monthly mean lapse rates of specific and relative humidity. Plots of seasonal and spatial humidity patterns illustrate the relations between humidity variables and temperature, elevation, and longitude in the region.

1. Introduction

Atmospheric humidity is under-studied relative to air temperature, but it has a strong influence on human, environmental, and ecological systems. There are several related measures of atmospheric humidity. Direct measures of the amount of water vapour include vapour pressure, e_v (hPa), specific humidity, q_v (g of vapour per kg of air), the mixing ratio, w (g of vapour per kg of dry air), and the absolute humidity or vapour density, ρ_v (g of water vapour per m^3 of air). Relative humidity, *RH*, is the most commonly reported humidity variable, but it is not a direct indication of the amount of water vapour. Rather, *RH* reports the amount of water vapour in air relative to the maximum amount of water that can be maintained as vapour at a given

temperature (i.e., the saturation content), usually expressed as a percentage. Once the air is saturated (RH = 100%), any additional vapour will condense out. For saturation vapour pressure $e_s(T)$, $RH = 100\, e_v / e_s$.

Each of these humidity variables is used in different contexts in meteorological, hydrological, biological, and ecological applications. Specific or absolute humidity is used to calculate total precipitable water in an air column, and to quantify water vapour transport in the atmosphere. These are also the appropriate variables to quantify the effects of humidity on incoming longwave radiation (i.e., the greenhouse effect of water vapour) (e.g., Ruckstuhl et al., 2007; Rangwala, 2013). In operational meteorology, the dry line is a term for strong horizontal gradients in specific humidity, a marker of air mass fronts associated with severe convective weather (e.g., Ziegler et al., 1997; Hoch and Markowski, 2005; Johnson and Hitchens, 2018). Applications of boundary layer meteorology to disciplines such as agriculture and hydrology also require humidity data, for calculation of turbulent latent heat fluxes from the near-surface gradient in specific humidity or vapour pressure (e.g., Marks and Dozier, 1992; Polonio and Soler, 2000).

Humidity also affects human comfort. Several indices combine temperature and humidity to provide a measure of heat stress under warm, humid conditions, such as the humidex (Masterson and Richardson, 1979), apparent temperature (Steadman, 1984), and the heat index (Epstein and Moran, 2006; Buzan et al., 2015). Vapour pressure deficit, the difference between saturation and actual vapour pressure ($e_s - e_v$), is an important meteorological variable in landscape ecology, where it serves as a proxy for moisture stress on vegetation (e.g., Eamus et al., 2013; Zuliani et al., 2015; Sanginés de Cárcer et al., 2017). Forest fire hazard is also linked to aridity, with relative humidity and vapour pressure deficit used as predictive variables in fire models (e.g., Pechony and Shindell, 2009; Silvestrini et al., 2011; Sedano and Randerson, 2014). Vapour pressure deficit is strongly associated with likelihood of ignition and burn area extent (Holden and Joly, 2011; Sedano and Randerson, 2014; Seager et al., 2015).

The amount of water vapour in the air is largely a property of the air mass and its provenance (e.g., maritime vs. continental air masses), modified by rainout and evapotranspiration from local moisture sources such as open water and croplands. Humidity fluctuations associated with different weather systems are superimposed on a seasonal cycle that is broadly controlled by temperature; saturation vapour pressure decreases exponentially in cold air, so specific humidity is lower in the winter season in the extratropics. In addition, there can be diurnal humidity cycles associated with daytime warming and evapotranspiration adding moisture to the near-surface air (e.g., Segal et al., 1992; Lengfeld and Ament, 2012), and overnight condensation which removes water vapour. Due to these processes, vapour pressure and specific humidity commonly increase during the day and decrease at night, while RH does the opposite. This can drive daytime convective instability in the warm season.

Spatial patterns of humidity and its variation across the landscape are less studied, particularly in mountain environments. Mesonets in the U.S. great plains provide a detailed view of the dryline (e.g., Ziegler et al., 1997; Hoch and Markowski, 2005), and specific humidity and dryline structures were examined in the Alberta foothills as part of the UNSTABLE field campaign in July 2008 (Taylor et al., 2011). The latter study reports higher specific humidity levels over agricultural croplands than the higher-elevation forested lands in the Alberta foothills. Johnson and Hitchens (2018) report similar findings in the U.S. Great Plains, where the dryline position is associated with soil moisture. Other systematic spatial humidity structures can be expected as a function of elevation, aspect, surface type, and air mass/frontal interactions.

This manuscript presents a dataset of humidity measurements over a large range of elevations and surface environments in the Rocky Mountain foothills in southern Alberta, Canada. The data are derived from a mesonet of 232 near-surface temperature and humidity loggers that were in place from 2005 to 2010, with the temperature data described in Wood et al. (2018a). The observations extend from prairie farmlands east of the city of Calgary to alpine sites along the continental divide of the Canadian Rocky Mountains, spanning elevations from 890-2880 m. Here we present the mean daily values of relative humidity, specific humidity, and vapour pressure over the five-year study. The dataset consists of 1826 days from 232 sites, giving a total of 423,362 records. Section 2 describes the study area and measurements in more detail, Sections 3 defines the humidity measures and discusses the calculation of daily mean values, Section 4 explains the quality control and gap-filling measures applied to the dataset, and Section 5 summarizes the mean monthly data, its spatial patterns, and lapse rates of humidity in the study region.

2. Study Area

The Foothills Climate Array (FCA) was established in 2004 and 2005 in the foothills of the Rocky Mountains in southwestern Canada, at approximately 51°N and 114.5°W (Figure 1). An area of roughly 18,000 km^2 (120 km × 150 km) was instrumented with a two-dimensional network of automatic weather stations recording temperature, relative humidity, and rainfall (Wood et al., 2018a). The FCA was set up in a series of east-west transects, spaced roughly 10 km apart and running from the continental divide on the western end of the study region to the flat, prairie grasslands on the eastern edge. Station spacing along the east-west transects was about 5 km in the mountains and 10 km for the sites with lower relief on the eastern half of the study region.

The continental divide runs northwest-southeast along the western margin of the FCA. Elevations of the high peaks in the Canadian Rocky Mountains reach 3500 m, with treeline at 2200-2600 m, depending on the aspect. The environment above treeline consists of rock, talus, alpine lakes, and glacier cover, with sparse vegetation. Coniferous forest and alpine meadows are found below the treeline, transitioning to mixed forest (e.g., aspen) in the lower-elevation rolling hills of the Alberta foothills. This grades into shrub, grassland, and cultivated cropland in the prairies, where land use changes to ranching,

Earth Syst. Sci. Data Discuss., https://doi.org/10.5194/essd-2018-62
Manuscript under review for journal Earth Syst. Sci. Data
Discussion started: 4 June 2018

farming, and urban areas. FCA sites are classified as mountain or prairie based on their elevation and terrain variability surrounding the site. Prairie sites are generally situated below 1250 m, with little terrain variability. Within this zone, nine sites are situated within the Calgary municipal boundary. Elevations drop to below 900 m at the eastern edge of the array. The study area and site locations therefore comprise a wide range of elevation, topography, and surface types.

Each FCA installation consisted of data-logging rainfall, temperature, and relative humidity gauges mounted on a pole that was either pounded into the ground or supported with a cairn. Temperature and relative humidity were recorded at 1-hour intervals, with instantaneous measurements taken at the top of the hour, using SP-2000 temperature-relative humidity data loggers manufactured by Veriteq Instruments Inc[1]. The data loggers were mounted inside radiation shields manufactured by Onset Scientific Ltd. to protect the loggers from direct sunlight and allow air circulation. The manufacturer-reported measurement range for the relative humidity sensors is 0 to 95%, with a 5-year accuracy of ±5% between 10% and 90% relative humidity at 25°C.

Up to 244 stations were in operation during the main recording period from July 2005 to June 2010, with 232 sites having reliable data. Site locations sampled the varying topography, land-surface types, and elevations of the study region (Wood et al., 2018a). Where possible, temperature and *RH* were recorded at a height of 1.5 m above the ground. At sites with significant snow accumulation (generally at elevations above 2000 m), pole extensions were added to keep the sensors above the winter snowpack and instrument heights were between 2 and 3 m. Sites do not conform to World Meteorological Organization (WMO) standards, which specify that climate recording sites should be level, away from vegetation and buildings, and not in areas of variable topography (WMO, 2008). This prescription is not consistent with the purpose of the study, which is to examine topographic and surface environmental influences on weather. By design, the array samples different slopes, aspects, and degrees of forest closure, to quantify realistic, landscape-scale spatial variability. Examples of site locations and more details on the FCA design are provided in Wood et al. (2018a).

3. Calculation of Daily Means

Calculation of mean daily humidity values can be complicated, due to the fact that *RH* is a constructed variable that depends non-linearly on both temperature and actual humidity. We take different approaches to this calculation. Mean daily temperature and relative humidity values can be computed from the arithmetic mean of hourly values, giving mean daily values that are true to the primary data. Following WMO (2008), saturation vapour pressure is calculated from:

$$e_s = 6.112 \exp\left(\frac{17.62T}{243.12+T}\right), \qquad T \geq 0℃; \tag{1a}$$

[1] Veriteq has subsequently been bought out by Vaisala, which continues to make an adapted version of this data logger.

Earth Syst. Sci. Data Discuss., https://doi.org/10.5194/essd-2018-62
Manuscript under review for journal Earth Syst. Sci. Data
Discussion started: 4 June 2018

$$e_s = 6.112 \exp\left(\frac{22.46T}{272.62+T}\right), \qquad T < 0℃, \tag{1b}$$

where T is the temperature in °C and the units of vapour pressure are hPa (mbar). These two expressions allow for the lower saturation vapour pressure over ice than over liquid water. Actual vapour pressure is then calculated from $e_v = e_s \cdot RH/100$. Given air pressure, P, specific humidity (g kg^{-1}), follows:

$$q_v = 622\left(\frac{e_v}{P-e_v}\right). \tag{2}$$

Using these equations, mean daily e_v and q_v can be calculated from the mean daily values of temperature, relative humidity, and air pressure. For a site with elevation z (m) and absolute temperature T_K, we estimate pressure based on the assumption of a standard atmosphere, using Environment Canada data from Calgary. The Calgary weather station has a reference elevation of z_0 = 1099 m. For reference temperature T_0 (K) and pressure P_0 (hPa), pressure at each site is calculated from the hypsometric equation (e.g., Wallace and Hobbs, 1977):

$$P(z) = P_0 \exp\left[\frac{-0.03416(z-z_0)}{0.5\cdot(T_K+T_0)}\right]. \tag{3}$$

Eq. (3) roughly accounts for the decrease in pressure with elevation, and can be calculated from either hourly or mean daily pressure in Calgary.

Vapour pressure and specific humidity values that are computed from mean daily T and RH values are not identical to the mean of hourly e_v and q_v data over the day, due to non-linearities in the saturation vapour pressure and the fact that RH saturates at 100%. Hence, we also calculate hourly e_v and q_v from the raw hourly T and RH data, then compute mean daily values of e_v and q_v from the arithmetic average of hourly data. This gives a truer estimate of these two measures of humidity. However, daily e_v and q_v calculated in this manner are not thermodynamically consistent with the mean daily values of T and RH. We anticipate that some applications of the data may require daily RH data and some will require actual humidity measures (e_v or q_v), so we present estimates of mean daily humidity derived from both methods. For applications that use actual humidity, we recommended using daily means based on the hourly e_v and q_v data, while being aware that these are not consistent with the mean daily T and RH. Differences in daily means calculated from the hourly or mean daily data are discussed further in Section 5.

Earth Syst. Sci. Data Discuss., https://doi.org/10.5194/essd-2018-62
Manuscript under review for journal Earth Syst. Sci. Data
Discussion started: 4 June 2018

4. Quality Control

4.1 Sensor Accuracy

Sensor calibration and quality control for the temperature data are described in detail in Wood et al. (2018a). For calibration tests, sensors were set to record instantaneous relative humidity at one, two, or five-minute intervals for one- to two-week periods. To represent the actual field methodology, top-of-the hour measurements were extracted for each sensor and compared with measurements at the University of Calgary weather research station (WRS), which uses a Campbell Scientific HMP35CF sensor mounted in a ventilated, Gill Model 41004-5 12 plate radiation shield. The reference site records data at one-minute intervals. To provide a direct comparison with our field measurements, we compare one-hour averages at the reference station with Veriteq data sampled at the top of hour. This gives an indication of how well the instantaneous top-of-hour measurements capture hourly average conditions.

Where the average *RH* difference between the sensor and the WRS is greater than 20%, we assume that the sensor is malfunctioning and we exclude these data. After rejecting these sensors, the average *RH* difference is less than 1% for all calibration studies carried out from 2004-2011. There is variability between sensors, with WRS-Veriteq differences having a standard deviation of 6% for all tests. Test results show that Veriteq sensors tend to read lower than the WRS during summer months and higher during winter months. Individual sensors have slightly different behaviour and some have biases of several %, although this may depend on the season of the sensor validation tests. Uncertainties in *RH* are estimated to be 6% for daily mean values, slightly greater than the instrumental accuracy. This 6% uncertainty propagates through to the estimates of vapour pressure and specific humidity. Compounded with the uncertainty of ±0.2°C in mean daily temperature (Wood et al., 2008a), through the calculation of saturation vapour pressure (Eq. 1), we estimate an accuracy of ±7% in mean daily e_v and q_v.

4.2 Quality Control (QC)

Erroneous temperature measurements from the Veriteq sensors are generally accompanied by unreliable relative humidity measurements. Therefore, *RH* data are excluded for the 9% of records with missing or faulty temperature measurements (see Wood et al., 2018a). Examination of the data indicates that relative humidity can also be erroneous at times with valid temperature data. Further quality control tests were therefore carried out to exclude additional bad data. While the range of the sensors is quoted as 0-95%, measurements in the field ranged from 0-100%. WRS relative humidity data ranged from 9-100% during the calibration tests. When the Veriteq sensors record humidity values less than 10%, the sensors commonly show limited variability through the day, likely indicating sensor malfunction. The study region is characterized by a dry, continental climate, but *RH* values below 10% are deemed to be physically unlikely. Hourly values less than 10% are therefore set to 10%. Next, data are excluded for days with the minimum value equal to the maximum value, when not equal to 100%. Additionally, we exclude days where values fluctuate between 10 and 100% repeatedly, or fluctuate and then flatline at either 10 or 100%.

Earth Syst. Sci. Data Discuss., https://doi.org/10.5194/essd-2018-62
Manuscript under review for journal Earth Syst. Sci. Data
Discussion started: 4 June 2018

The final quality assessment test compares site daily mean and minimum values with the average mean and minimum values calculated from a group consisting of the 30 nearest neighbour stations. Daily maxima are not used as it was common for days to have 100% as the maximum value. Neighbourhood means exclude sites with questionable data, based on sensors that failed any of our QC tests and days with less than 20 hours of measurements. In addition, the site(s) within a group having the lowest or highest daily mean and minimum values are excluded from the neighbourhood means calculation. This step is meant to filter out anomalous local effects, which may be real but can be specific to local conditions. Site-days where either the minimum or mean value exceeds the neighbourhood mean or minimum by more than 3 standard deviations are excluded from the final dataset.

The quality control steps results in exclusion of ~2% of the data, in addition to the data that are rejected due to missing or faulty temperature readings. The final dataset is 89% complete, but missing data affect more than 90% of the sites. We therefore estimate missing data to make for more straightforward and reliable applications of this dataset.

4.3. Gap-Filling of Missing Data

Our dataset presents daily mean (vs. hourly) meteorological conditions, so we designed our quality-control and gap-filling algorithms to estimate daily mean values. For the 89% of site-days with valid data, daily humidity measures calculated directly from hourly temperature, relative humidity, and pressure. Where complete daily data are unavailable, we gap-fill these days using spatial interpolation of mean daily data from neighbouring sites. Temperature data used for the humidity calculations is complete, based on gap-filling strategies detailed in Wood et al. (2018a).

Spatial interpolation methods such as inverse distance weighting (IDW) or kriging can be used to interpolate spatially autocorrelated data (e.g., Ozelkan et al., 2015). For large areas with small variations in topography, a combination of multiple regression using horizontal location and elevation- and inverse distance-squared weighted interpolation (Gradient Inverse Distance Squared or GIDS) has been used by Nalder and Wein (1998). However, there is variable topography in the FCA area and humidity can vary systematically with elevation, so this method is not suitable. Co-kriging, as used by Ishida and Kawashima (1993), explicitly controls for elevation by including elevation as a co-variate. Apaydin et al. (2004) apply co-kriging with elevation for interpolation of different meteorological variables in southeastern Turkey. They recommend co-kriging for spatial interpolation of most variables, including *RH*.

Using Equations (1)-(3), q_v can be calculated from *T*, *RH*, and *P*. Spatial interpolation can be applied to either q_v or *RH* to estimate missing values. The other humidity variable is then calculated from the estimated value. In this study we tested IDW and kriging methods on both daily mean q_v and *RH*. Both datasets exhibit positive spatial auto-correlation, with *RH* showing no correlation with elevation and q_v moderately correlated with elevation. Leave-one-out cross validation for 2006 data, the

most complete full year of data, is used to determine the best method and parameters to estimate missing data. With this method, the model is run as many times as there are data points, excluding a different data point for each run, and the remainder of the data are used to estimate the removed point. Using cross-validation, various error measures can be calculated by comparing predicted and observed values, e.g., root mean square errors (RMSE) and mean absolute errors (MAE).

The IDW technique considers a number of points within a neighbourhood of the target location, with contributions weighted inversely according to the distance between each point and the site of interest. The rate of decay can be varied by applying a power function to the separation distance. Higher powers increase the weighting of nearby points relative to more distant points. Kriging also considers a number of points within a neighbourhood, but the relative contributions are based on a semi-variogram, which models the distance/variance function calculated from all points within a predefined range. The co-kriging model included elevation as a co-variate with q_v, where neighbourhood weights are based on a cross-semivariogram modelled on the covariance between elevation and q_v.

4.3.1 Inverse Distance Weighting (IDW)

IDW interpolation models were run for each day, leaving each site out in turn and using the remaining sites to predict the omitted site. Models were run with the power parameter varying from 1 to 3.5 in 0.25 increments and using between 5 and 30 neighbours. Errors are calculated as the difference between the estimated and measured values. The MAE and RMSE are calculated for the 2006 data for each combination of power and number of neighbours. Interpolating q_v and then calculating *RH* generates some unrealistic *RH* values, greater than 100%. In this event, *RH* is set to 100% and q_v is recalculated. This gives physically consistent values of q_v, temperature, pressure, and *RH*.

4.3.2 Kriging

The semi-variogram models the variance between humidity measures for all site-pairs as a function of separation distance. The spatial relationship can be modelled using different functions e.g. spherical or exponential, and varying the values for the sill, nugget and range parameters (e.g., Isaaks and Srivastava, 1989). The range represents the limit of correlation between sites, the sill represents the maximum variance between sites, and the nugget represents the minimum variance between close sites. The semi-variogram function groups sites into bins based on separation distance, and the variance between sites can differ on a daily basis. Semi-variogram models were produced for annual aggregated data (annual mean value for each site), monthly aggregated data (mean monthly value for each site), and for daily data. These models are used to estimate each site/day using leave-one-out cross-validation.

Differences in mean errors are small for the different interpolation methods (IDW and kriging), variables (q_v and *RH)* and model parameters. The model with the lowest errors for both q_v and *RH* uses IDW interpolation with a power of 2. For specific humidity, the optimal results are for 18 neighbours. This is the method chosen to estimate the missing data.

Earth Syst. Sci. Data Discuss., https://doi.org/10.5194/essd-2018-62
Manuscript under review for journal Earth Syst. Sci. Data
Discussion started: 4 June 2018

Open Access Earth System Science Data Discussions

5. Results and Discussion

5.1. Calculation of Daily Means

Mean daily specific humidity was calculated from two different methods: (i) q_{vd}, calculated from Eqs. (1)-(3) using mean daily T and RH values, and (ii) q_{vh}, from the arithmetic average of hourly e_v and q_v (i.e., based on the hourly T and RH data). Results are not identical due to non-linearities in the saturation vapour pressure and the fact that RH saturates at 100%.

Differences between these two methods are plotted in Figure 2 for all site-days as a function of mean daily temperature and daily temperature range. Differences are greatest for higher temperatures and when the diurnal temperature range is large. On days where the mean temperature is greater than 15°C, the average q_v difference, $\Delta q_v = q_{vd} - q_{vh}$, is equal to 0.3 g kg^{-1}. Saturation vapour pressure increases exponentially with temperature, so the maximum possible specific humidity during the cool hours of a day (typically overnight) is limited, and is commonly an order of magnitude or more less than during the warmest hours of the day. On days with a large diurnal temperature range, low overnight values of q_v tend to decrease the average daily specific humidity calculated from method (ii). Hence, Δq_v is generally positive, and increasingly so on warm days with a high diurnal range. This is also true for the percentage difference (Figure 2), where Δq_v has a roughly relationship with both temperature and diurnal temperature amplitude across the full range of observed conditions (with exceptions to this behaviour). Relative differences vary from −10 to +10%. Absolute differences are generally less than 0.1 g kg^{-1} on cold days ($T < -5$°C), as specific humidity is low.

The hourly data gives a truer estimate of daily mean vapour pressure and specific humidity: this is the most correct estimate of how much water vapour is present on a given day. These values are recommended for applications that require daily mean values, such as estimates of precipitable water, parameterizations of incoming longwave radiation (Brutsaert, 1975; Sedlar and Hock, 2009), or latent heat flux calculations in boundary layer meteorology (e.g., Oke, 1987; Andreas, 2002). However, we recognize that these values of e_v and q_v are not thermodynamically consistent with the daily mean values of T and RH in our dataset. Hence, we also provide daily mean estimate of e_v and q_v based on the daily average temperature and RH. These are recommended for some applications, e.g. those which use vapour pressure deficit, which require estimates of e_s from mean daily temperature.

5.2. Gap-Filled Data

About 11% of the values in this dataset are gap-filled to give a clean dataset with complete temporal and spatial coverage. Errors associated with the spatial interpolation methods are assessed at known sites, based on jackknife (leave-one-out) techniques. We tested different interpolation methods for both q_v and RH, to examine which field gives the lowest errors under interpolation. The resulting values are then used to calculate the other unknown (either q_v or RH); this is again required for

Earth Syst. Sci. Data Discuss., https://doi.org/10.5194/essd-2018-62
Manuscript under review for journal Earth Syst. Sci. Data
Discussion started: 4 June 2018

thermodynamic consistency, as independent interpolations of both q_v and *RH* at a site give values that are inconsistent with the daily mean temperature.

The lowest errors in our dataset are with IDW interpolation of q_v. Table 1 summarizes the standard error of the interpolation for mountain and prairie sites and as a function of season. Average interpolation errors for q_v are 0.3 g kg^{-1}, and 90% of estimated q_v values are within ±0.5 g kg^{-1} of the actual values. Errors are greater for the mountain sites than in the prairies, and absolute errors increase with warmer temperatures, from 0.2 g kg^{-1} in winter to 0.5 g kg^{-1} in summer. Relative (percentage) error has the opposite relationship but is relatively constant year-round, at 10% in the winter months and 6% in the summer. Interpolation errors in *RH* average 5%, with 90% of values in the range –12 to +10%. Similar to q_v, average errors at mountain sites are twice as large as in the prairies (6% vs. 3%) and relative errors are slightly higher in the winter season.

For both q_v and *RH*, the mean error in the interpolation is about 7% of the mean annual values, 4.4 g kg^{-1} and 72% (see Table 2), with errors of about 6% and 10% in the summer and winter seasons, respectively. Based on the 5th and 95th percentiles (Table 1), 90% of q_v and *RH* values have errors of less than 11% and 15%, respectively. It is difficult to select which humidity variable is better to interpolate based on these results, although q_v is intuitively favorable since it is a continuous variable and an actual physical field, rather than a construct of two different variables (temperature and actual humidity), with a saturation point (100%). As an additional test, Figure 3 plots the frequency distribution of actual and interpolated q_v and *RH* values. The two-sample Kolmogorov–Smirnov test determines whether two samples have similar cumulative probability distribution functions. Estimated and actual q_v values are statistically similar at the 95% significance level, but *RH* values differ. These differences are visible in Figure 3, and support the case for interpolating specific humidity rather than *RH*. This is the approach we adopt to fill data gaps, with daily mean e_v and *RH* calculated from *T* and interpolated q_v.

5.3. Seasonal and Spatial Humidity Variations

Table 2 summarizes the monthly mean values of temperature and each humidity variable over the study area. Spatial variability across the FCA is represented through the standard deviation in each value (N = 232). These monthly values neglect the spatial richness of the dataset, but they illustrate the mean climatology and seasonal cycle of the humidity variables in this region, for the period 2005-2010. For reference, the average elevation of FCA sites is 1480 m.

Relative humidity has a moderate seasonal cycle, averaging 70% in summer (JJA) and 75% in winter (DJF), with greater spatial variability in the study region in the winter months (±5% and ±8% for the two seasons, respectively). Vapour pressure and specific humidity are strongly correlated, so we primarily discuss the latter. These two variables have a strong seasonal cycle, associated with temperature controls on atmospheric moisture and increased warm-season evapotranspiration. Mean

winter and summer values for q_v are within 2.0 and 7.7 g kg^{-1}, respectively, with a maximum in July. Spatial variability is much greater in the warm season, increasing from 5% in the winter to 12% in the summer.

Figure 4 plots the spatial distribution of mean seasonal q_v across the study region. This illustrates the relatively low spatial variance in winter. Locations in the foothills that are slightly drier in the winter season may be capturing the regional chinook belt (Nkemdirim, 1996; Cullen and Marshall, 2011), which runs northwest-southeast in the lee of the Rocky Mountains. The other three seasons are characterized by strong longitudinal and altitudinal gradients in specific humidity, with more humid conditions on the lower-elevation, agricultural lands in the eastern section of the FCA. The City of Calgary has no apparent influence on humidity patterns. In the autumn and winter, there is evidence of humid Pacific air masses that cross over the continental divide into the western part of the study area, particularly in the central region. The Bow River is also evident in these plots at the mountain sites, running eastwards along FCA lines 3 and 4, where line 1 is the northernmost line (see Figure 1). More humid conditions are recorded at sites adjacent to the river, typically ~1 g kg^{-1} greater than neighbouring sites to the north and south. This indicates that the river provides a significant local source of near-surface moisture in the mountains. This influence is not discernible at the more humid prairie sites.

Figure 5 plots the seasonal relation between specific humidity, elevation, and longitude in the study region. Vertical gradients ('lapse rates') of q_v and *RH* are given in Table 2, calculated from a linear regression of mean monthly values vs. elevation. Consistent with Figure 4, there is no relationship between specific humidity and elevation in the winter months. There is a strong elevational dependence from March through October, however, with significant regressions ($p < 0.01$) and R^2 values greater than 0.8 in all cases. The mean specific humidity lapse rate in summer is –2.1 g kg^{-1} km^{-1}, a strong decrease in specific humidity with elevation. Relative to the mean summer value of 7.7 g kg^{-1} in the study area, this is a decline of 27% per 1000 m of elevation. Specific humidity lapse rates in autumn and spring are also significant, but weaker (~17% per 1000 m). Autumn has more scatter (Figure 5a), probably because September is transitional between summer and autumn weather patterns in the study region.

Relative humidity has a weaker relationship with elevation than q_v from March through October, with variable sign and lower R^2 values (Table 2). In contrast, there is a significant relationship from November through January, with an average vertical gradient of +5.6% km^{-1}. This indicates conditions closer to saturation at higher elevations in the study area. This is the general tendency year-round and is particularly strong in April and May (+8.3% km^{-1}). July and August offer interesting exceptions, with an average relative humidity lapse rate of –4.5% km^{-1}. Higher elevations are drier in these peak summer months with respect to both specific and relative humidity. The result may reflect the strong evapotranspirative moisture source in the grass- and croplands at lower elevations in the study area in the summer (Taylor et al., 2011). Variations in specific humidity with longitude plotted in Figure 5b also support this. It is difficult to separate the effects of elevation vs. longitude in the data, as

Earth Syst. Sci. Data Discuss., https://doi.org/10.5194/essd-2018-62
Manuscript under review for journal Earth Syst. Sci. Data
Discussion started: 4 June 2018

Open Access Earth System Science Data Discussions

these are strongly correlated (r = –0.80), and both spatial variables are related to potential moisture sources in the agricultural croplands on the eastern portion of the study area.

Humidity patterns in the FCA region also reflect the regional temperature structure, associated with thermodynamic limits on the amount of water vapour and the influence of temperature on *RH* (saturation). Figure 6 plots mean annual e_v, q_v, and *RH* vs. temperature at each FCA site, based on the five-year averages. There is a significant relation with temperature for each variable, with e_v and q_v decreasing with temperature and *RH* increasing. This accounts for much of the observed elevation dependence.

Daily humidity structure can be much more complex than the seasonal and annual mean patterns. Different air masses impact the study region, associated with synoptic- and regional-scale weather patterns that cover all or part of the FCA on a given day. Examples include extratropical cyclones that can stall against the mountain barrier, advecting mild, humid air from the southeast (e.g., Milrad et al., 2015), continental polar air masses from the north (Cullen and Marshall, 2011), chinook conditions that can occur under strong westerlies (Nkemdirim, 1996), and hot summer days that give rise to local- to regional-scale convective instability (Taylor et al., 2011). The latter commonly manifest as late afternoon thunderstorms, in association with dryline development in the northern part of the study area. Each of these weather types can be expected to have characteristic humidity patterns.

As examples, Figure 7 shows daily mean q_v and *RH* structure across the FCA for each of the weather systems outlined above. The cyclonic system in Figures 7a and 7b gives a good representation of elevation/temperature controls on specific humidity, as *RH* is ~100% over the entire domain. Cloud cover and precipitation extend over the region and there is a strong source of moisture advection, so there are primarily thermodynamic constraints on specific humidity (saturation). The example in Figures 7c and 7d is for a hot summer day with localized thunderstorm activity. In this case there is a strong contrast between mountain and prairie sites, and q_v and *RH* are highly correlated. Evapotranspiration in the prairie croplands may be providing a source of near-surface moisture on the eastern portion of the domain. The high humidity levels are notably absent in the City of Calgary. Daily mean structure is interesting for this case, but analyses of convective instability and the dryline would be better served with the hourly data, which are beyond the scope of this dataset and manuscript.

The lower four panels in Figure 7 are for winter weather systems. These illustrate the contrasting influences of a cold, continental air mass that pushes into the region from the northeast (Figures 7e and 7f) and chinook winds from the west (Figures 7g and 7h). In both cases there is a general “inversion” structure in the humidity relationships with elevation, in contrast to the two summer systems in the top four panels. The continental polar air mass that sits over the prairies in Figures 7e and 7f is cold ($T \approx -20$°C), dry ($q_v < 2$ g kg^{-1}), and near saturation, with $RH \approx 90$%. Conditions are exceptionally uniform over the prairies and foothills. The western section of the study area contrasts sharply, and is under the influence of a westerly (Pacific) air mass on this day. This brought mixed rain and snow to the mountain sites on this day, with specific humidities of ~5 g kg^{-1}

and an average temperature of 0.7°C in Banff, Alberta. There is a clear transition zone in the foothills separating the Pacific and Arctic air masses, with intermediate values of q_v and lower *RH*.

The chinook day in Figures 7g and 7h has some common structure, particularly the low specific humidity in the prairies and foothills. In this case only the westernmost sites have higher humidity values, and most of the domain has both low q_v (< 2 g kg^{-1}) and *RH* (< 50%). Chinook winds are associated with dry-adiabatic descent in the lee of the Rockies, bringing warm and dry conditions. Figures 7g and 7h are a classical example of this, with the chinook belt evident over an ~80-km wide swath that parallels the continental divide. High-elevation sites near the continental divide are experiencing cloud cover, strong winds, and intermittent precipitation. Chinook effects weaken east and north of Calgary, with higher q_v and *RH*. Conditions like these two winter examples are frequent in the cold season, with moist Pacific air masses penetrating over the continental divide and reaching high-elevation sites on the western portion of the grid. The contrast with cold, dry continental air over the prairies creates a humidity inversion with altitude.

The examples in Figure 7 demonstrate the richness of dataset and its potential value for different meteorological, ecological, hydrological, and agricultural applications. While there is systematic structure in the seasonal and annual humidity patterns, daily humidity patterns can deviate strongly from this. Additional studies are needed to analyse the interaction of weather systems with terrain and surface cover in the study region, but humidity patterns can help to understand this interaction. These examples also reveal the importance of considering daily weather systems as well as seasonal cycles in algorithms which downscale humidity distributions over the terrain, e.g., from climate model reanalyses or projections (e.g., Abatzoglou, 2013; Pierce and Cayan, 2016).

6. Data availability

Data described are available on the PANGAEA repository https://doi.pangaea.de/10.1594/PANGAEA.889435 (Wood et al., 2018b), with links to the temperature data (Wood et al., 2017). Mean daily temperature, pressure, vapour pressure, relative humidity, and specific humidity data are available at each of the 232 sites for the period July 1, 2005 to June 30, 2010. Site latitude, longitude, elevation, land surface type, and sensor height above ground are also noted, and there is a flag to mark whether humidity data for each site-day are directly measured or estimated (interpolated). Where measured data are available, we provide vapour pressure and specific humidity estimates using two different ways to calculate daily means, as described in the text (see Section 5.1).

Earth Syst. Sci. Data Discuss., https://doi.org/10.5194/essd-2018-62
Manuscript under review for journal Earth Syst. Sci. Data
Discussion started: 4 June 2018

7. Summary

The Foothills Climate Array (FCA) offers a unique collection of high-density, multi-year observations in complicated mountain terrain. These data provide a detailed view of near-surface humidity patterns and their temporal variability. This manuscript presents the dataset, quality-control and gap-filling strategies used to process the data, and basic characteristics of the dataset, including monthly means of specific and relative humidity and their relation with temperature, elevation, and longitude in the study area. We include examples of daily humidity patterns under different weather systems, to illustrate the complex but systematic interactions between the surface environment, topography, air masses, and meteorological processes in this region. The FCA temperature and humidity data are valuable for a range of applications in fields such as ecological or hydrological modelling, and can also help to inform climate downscaling strategies in mountain terrain.

The Veriteq relative humidity instruments used in this study performed well, with some variability between sensors. Validation experiments against a reference sensor indicate an average bias of less than 1% but a standard error (uncertainty) of ±6% in the field measurements or relative humidity, slightly greater than the factory-reported sensor accuracy. This propagates through to calculations of daily mean vapour pressure and specific humidity, increasing the uncertainty to ±7% when accounting for the uncertainty in temperature measurements.

Errors of a similar magnitude result from the method chosen to calculate daily means, but in this case the errors can be systematic (i.e., a consistent bias). Specifically, specific humidity calculated using mean daily T and RH can deviate by up to ±10% from the "true" daily means that are calculated using hourly data. This effect is greatest for high temperatures and when there is a large diurnal temperature range. For mean daily temperatures of −10°C to +10°C, the effect is less than 3%. This result is due to nonlinearities in the saturation vapour pressure curve with temperature as well as threshold effects, where RH saturates at 100%. We present daily mean e_v and q_v using both methods: (i) hourly means of e_v and q_v and (ii) daily means calculated from mean daily T and RH. The former are recommended as they provide a better estimate of actual water vapour over the day, but we wish to point out that the resulting values of mean daily e_v and q_v are not thermodynamically consistent with the mean daily T and RH.

Quality control procedures were successful in identifying and removing questionable data. In total, 11% of data collected at the 232 sites between 2005 and 2010 are missing or unreliable. Missing and unreliable data are distributed randomly in the study area. While the dense station network provides some redundancy and the percentage of missing data is not high, gap-filling to create a complete dataset has benefits for applications requiring monthly means or for creating interpolated humidity surfaces. We therefore gap-filled the data that are available here using spatial interpolation, with a flag to denote data that have been estimated. Validation of our gap-filling method for sites with known data indicates average errors of ±7% in the

interpolated q_v and *RH* data. Errors are higher in the winter (±10%). Optimal spatial interpolation results in our dataset are for inverse-distance weighting of specific humidity, with a neighbourhood of 15 sites.

Monthly mean specific and relative humidity have strong relations with temperature, elevation, and longitude in our study area. Sites on the eastern portion of our grid have higher specific humidity in all seasons but winter, with the strongest contrasts in the summer. High summer humidity may be associated with evapotranspirative moisture sources in the grass- and croplands in this area. The western half of the FCA region is at higher elevation and is dominated by forested and alpine landscapes. Cooler temperatures in the mountains and the resulting constraints on saturation vapour pressure also explain part of the longitudinal variation, particularly in the spring and autumn. The average annual specific humidity gradient with elevation is -0.85 g kg^{-1} km^{-1}, reflecting the cooler, drier air at higher altitudes. This also creates a general increase in *RH* with altitude, with an average gradient of +3% km^{-1}.

Depending on the weather system and air mass that are in the region, spatial humidity patterns in the daily data can diverge markedly from the average seasonal and annual patterns. This is a significant challenge for downscaling or interpolating humidity fields in complex terrain. For applications requiring daily data, it may be fruitful to consider humidity structure as a function of the prevailing weather system. As an intermediate step to resolve some of the systematic spatial and temporal humidity structure, downscaling of humidity fields could be done using monthly or seasonal elevation gradients (lapse rates). Specific humidity lapse rates have a strong seasonal cycle. Summer lapse rates average -2.1 g kg^{-1} km^{-1}, spring and autumn values average -0.7 g kg^{-1} km^{-1}, and there is no relation between specific humidity and elevation from November through February, due to frequent humidity inversions in the study region. Relative humidity has less defined seasonal patterns, and the relationship with elevation changes sign in different months. *RH* decreases with altitude in the study area during July and August, possibly reflecting the local sources of near-surface moisture at low-elevation sites. For interpolation and downscaling of humidity fields, we recommend working with specific humidity and temperature, then calculating relative humidity from the these as more primary physical variables.

Acknowledgements

The Foothills Climate Array was funded by the Canada Foundation for Innovation, the Natural Sciences and Engineering Research Council (NSERC) of Canada, and the Canada Research Chairs program. We thank Rick Smith at the University of Calgary weather research station for his invaluable help over the lifetime of the FCA study. Graduate and undergraduate students, summer research assistants, friends, and volunteers that contributed to the FCA study are too numerous to list, but prominent within this group are Terri Whitehead, Kara Przeczek, and Bridget Linder. We could not have managed this study without their dedication and enthusiasm.

References

Andreas, E. L.: Parameterizing scalar transfer over snow and ice: a review, J. Hydrometeorol., 3, 417-432, 2002.

Apaydin, H., Sonmez, F.K. and Yildirim, Y.E.: Spatial interpolation techniques for climate data in the GAP region in Turkey. Clim. Res., *28*(1), 31-40, 2004.

Abatzoglou, J.T.: Development of gridded surface meteorological data for ecological applications and modelling. Int. J. Climatol., 33, 121-131, doi:10.1002/joc.3413, 2013.

Brutsaert, W.: On a derivable formula for long-wave radiation from clear skies. Water Resour. Res., 11, 742–744, 1975.

Buzan, J. R., Oleson, K. and Huber, M.: Implementation and comparison of a suite of heat stress metrics within the Community Land Model version 4.5. Geosci. Model Dev., 8, 151-170, doi:10.5194/gmd-8-151-2015, 2015.

Cullen, R. M. and Marshall, S. J.: Mesoscale temperature patterns in the Rocky Mountains and foothills region of southern Alberta. Atmosphere-Ocean, 49 (3), 189-205, doi:10.1080/07055900.2011.592130, 2011.

Eamus, D., Boulain, N, Cleverly, J., and Breshears, D.D.: Global change-type drought-induced tree mortality: vapor pressure deficit is more important than temperature per se in causing decline in tree health, Ecology and Evolution, 3 (8), 2711-2729, doi:10.1002/ece3.664, 2013.

Epstein, Y. and Moran, D. S.: Thermal comfort and the heat stress indices, Indust. Health, 44, 388–398, 2006.

Environment Canada, http://climate.weather.gc.ca/climate_data/daily_data_e.html?StationID=50430. Historical climate data for Calgary International Airport, last access 2 November 2015.

Hoch, J. and Markowski, P.: A climatology of springtime dryline position in the U.S. Great Plains region. J. Climate, 18, 2132-2137, 2005.

Isaaks, E.H. and Srivastava, R.M.: An Introduction to Applied Geostatistics. Oxford University Press, New York, 1989.

Johnson, Z.F. and Hitchens, N.M.: Effects of soil moisture on the longitudinal dryline position in the southern Great Plains. J. Hydrometeor., 19, 273–287, https://doi.org/10.1175/JHM-D-17-0091.1, 2018.

Marks, D., and Dozier, J.: Climate and energy exchange at the snow surface in the alpine region of the Sierra Nevada. 2. Snow cover energy balance. Water Resour. Res., 28, 3043– 3054, 1992.

Masterson, J. M. and Richardson, F. A.: Humidex, a method of quantifying human discomfort due to excessive heat and humidity, Environment Canada, Atmospheric Environment Service, Downsview, Ontario, CLI 1-79, 1979.

Milrad, S.M., Gyakum, J.R. and Atallah, E.H.: A meteorological analysis of the 2013 Alberta flood: Antecedent large-scale flow pattern and synoptic–dynamic characteristics. Mon. Wea. Rev., 143, 2817–2841, https://doi.org/10.1175/MWR-D-14-00236.1, 2015.

Nkemdirim, L.: Canada's chinook belt. Int. J. Climatol., 16 (4), 441-462, 1996.

Oke, T.R.: Boundary Layer Climates, 2nd Ed, Psychology Press, New York, 435, 1987.

Ozelkan, E., Bagis, S., Ozelkan, E.C., Ustundag, B.B., Yucel, M. and Ormeci, C.: Spatial interpolation of climatic variables using land surface temperature and modified inverse distance weighting, Int. J. Rem. Sens., 36 (4), 1000-1025, 2015.

Pechony, O. and Shindell, D. T.: Fire parameterization on a global scale, J. Geophys. Res.-Atmos., 114, D16115, doi:10.1029/2009JD011927, 2009.

Pierce, D.W. and Cayan, D.R.: Downscaling humidity with Localized Constructed Analogs (LOCA) over the conterminous United States. Clim. Dyn., 47 (1-2), 411-431, doi:10.1007/s00382-015-2845-1, 2016.

Polonio, D. and Soler, M.: Surface fluxes estimation over agricultural areas. Comparison of methods and the effects of land surface inhomogeneity. Theor. Appl. Climatol., 67, 65-79, doi:10.1007/s007040070016, 2000.

Rangwala, I.: Amplified water vapour feedback at high altitudes during winter. Int. J. Climatol., 33, 897-903, doi:10.1002/joc.3477, 2013.

Ruckstuhl, C., Philipona, R., Morland, J. and Ohmura, A.: Observed relationship between surface specific humidity, integrated water vapor, and longwave downward radiation at different altitudes. J. Geophys. Res., 112, D03302, doi:10.1029/2006JD007850, 2007.

Sanginés de Cárcer, P., Vitasse, Y., Peñuelas, J., Jassey, V. E. J., Buttler, A. and Signarbieux, C.: Vapor-pressure deficit and extreme climatic variables limit tree growth. Global Change Biol., doi:10.1111/gcb.13973, 2017.

Seager, R., Hooks, A., Williams, A. P., Cook, B., Nakamura, J. and Henderson, N.: Climatology, variability, and trends in the U.S. vapor pressure deficit, an important fire-related meteorological quantity. J. App. Met. Climatol., 54 (6), 1121-1141, doi:10.1175/JAMC-D-14-0321.1, 2015.

Sedano, F., and Randerson, J. T.: Multi-scale influence of vapor pressure deficit on fire ignition and spread in boreal forest ecosystems. Biogeosciences, 11 (14), 3739-3755, doi:10.5194/bg-11-3739-2014, 2014.

Sedlar, J. and Hock, R.: Testing longwave radiation parameterizations under clear and over-cast skies at Storglaciren, Sweden. Cryosphere, 3, 75-84, doi:10.5194/tc-3-75-2009, 2009.

Silvestrini, R. A., Soares, B. S., Nepstad, D., Coe, M., Rodrigues, H., and Assuncao, R.: Simulating fire regimes in the Amazon in response to climate change and deforestation, Ecol. Appl., 21, 1573–1590, 2011.

Steadman, R. G.: A universal scale of apparent temperature, J. Climatol. Appl. Meteorol., 23, 1674–1687, 1984.

Taylor, N.M., Sills, D.M., Hanesiak, J.M., Milbrandt, J.A., Smith, C.D., Strong, G.S., Skone, S.H., McCarthy, P.J. and Brimelow, J.C.: The Understanding Severe Thunderstorms and Alberta Boundary Layers Experiment (UNSTABLE) 2008. Bull. Amer. Meteor. Soc., 92 (6), 739–763, https://doi.org/10.1175/2011BAMS2994.1, 2011.

Wallace, J.M. and Hobbs, P.V.: *Atmospheric Science: An Introductory Survey*. Academic Press, 55–57, 1977.

World Meteorological Organization: Guide to meteorological instruments and methods of observations. 7th edition. World Meteorological organization, Geneva, Switzerland, 2008.

Wood, W. H., Marshall, S. J., Fargey, S. E., and Whitehead, T.L.: Daily temperature data from the Foothills Climate Array mesonet, Canadian Rocky Mountains, 2005–2010, PANGAEA, https://doi.org/10.1594/PANGAEA.880611, 2017.

Wood, W. H., Marshall, S. J., Whitehead, T. L., and Fargey, S. E.: Daily temperature records from a mesonet in the foothills of the Canadian Rocky Mountains, 2005–2010, Earth Syst. Sci. Data, 10 (1), 595-607, doi:10.5194/essd-10-595-2018, 2018a.

Wood, W. H., Marshall, S. J., Fargey, S. E., and Whitehead, T.L.: Near-surface atmospheric humidity data from a mesoscale meteorological network in the foothills of the Canadian Rocky Mountains, 2005-2010. PANGAEA, https://doi.pangaea.de/10.1594/PANGAEA.889435, 2018b.

Ziegler, C. L., Lee, T. J. and Pielke Sr., R. A.: Convection initiation at the dryline: A modeling study. Mon. Weath. Rev., 125**,** 1001-1026, 1997.

Zuliani, A., Massolo, A., Lysyk, T., Johnson, G., Marshall, S., Berger, K. and Cork, S.C.: Modelling the northward expansion of Culicoides Sonorensis (Diptera Ceratopogonidae) under future climate scenarios. PLoS ONE, 10 (8), e0130294, doi:10.1371/journal/pone.0130294, 2015.

Earth Syst. Sci. Data Discuss., https://doi.org/10.5194/essd-2018-62
Manuscript under review for journal Earth Syst. Sci. Data
Discussion started: 4 June 2018

Open Access Earth System Science Data Discussions

Tables and Figures

				Station class		Season			
				mountain	prairie	DJF	MAM	JJA	SON
	σ_e	0.05	0.95	σ_e	σ_e	σ_e	σ_e	σ_e	σ_e
q_v (g kg^{-1})	0.3	–0.5	0.5	0.4	0.2	0.2	0.3	0.5	0.3
RH (%)	5	–12	10	6	3	6	5	4	5

Table 1. Spatial interpolation errors for q_v and *RH* by station class (mountain vs. prairie site) and season. σ_e is the standard error estimate and 0.05 and 0.95 are the 5th and 95th percentile values of the error, respectively.

(a)	*T* (°C)	*RH* (%)	e_v (hPa)	q_v (g kg^{-1})	**(b)**	β_{RH} (% km^{-1})	β_{q_v} (g kg^{-1} km^{-1})
Jan	–6.4 ± 1.8	75 ± 9	2.9 ± 0.2	2.1 ± 0.1		*4.9*	–0.02
Feb	–6.3 ± 1.3	71 ± 6	2.6 ± 0.2	1.9 ± 0.1		–1.3	–0.04
Mar	–2.7 ± 2.2	73 ± 7	3.7 ± 0.5	2.7 ± 0.2		*4.7*	*–0.44**
Apr	1.2 ± 2.5	68 ± 5	4.6 ± 0.6	3.4 ± 0.3		*7.8**	*–0.65**
May	6.9 ± 2.9	69 ± 5	6.8 ± 1.0	5.0 ± 0.5		*8.9**	*–1.02**
Jun	10.6 ± 2.7	70 ± 4	9.3 ± 1.6	6.7 ± 0.8		*2.4*	*–1.82**
Jul	15.0 ± 2.3	69 ± 5	12.0 ± 2.1	8.7 ± 1.2		*–5.2*	*–2.51**
Aug	12.6 ± 2.1	72 ± 5	10.6 ± 1.7	7.7 ± 0.8		*–3.8*	*–1.85**
Sep	8.6 ± 2.1	69 ± 5	7.9 ± 1.0	5.7 ± 0.5		0.6	*–1.08**
Oct	2.4 ± 2.1	75 ± 6	5.5 ± 0.6	4.0 ± 0.3		*5.1*	*–0.53**
Nov	–2.6 ± 2.0	71 ± 9	3.6 ± 0.3	2.7 ± 0.2		*7.9*	*–0.17*
Dec	–9.1 ± 1.7	79 ± 8	2.5 ± 0.2	1.9 ± 0.1		*4.0*	–0.00
Annual	2.5 ± 2.0	72 ± 5	6.0 ± 0.8	4.4 ± 0.4		*2.9*	*–0.85**

Table 2. (a) Monthly means and standard deviations of temperature, relative humidity, vapour pressure and specific humidity across all FCA sites. Standard deviation refers to the spatial variability in mean monthly values. (b) Mean monthly lapse rates of relative and specific humidity, assuming a linear relationship with elevation: $\beta_{RH} = dRH/dz$ and $\beta_{q_v} = dq_v/dz$. Italicized values are statistically significant ($p < 0.01$) and asterisks indicate regressions with $R^2 > 0.4$.

Earth Syst. Sci. Data Discuss., https://doi.org/10.5194/essd-2018-62
Manuscript under review for journal Earth Syst. Sci. Data
Discussion started: 4 June 2018

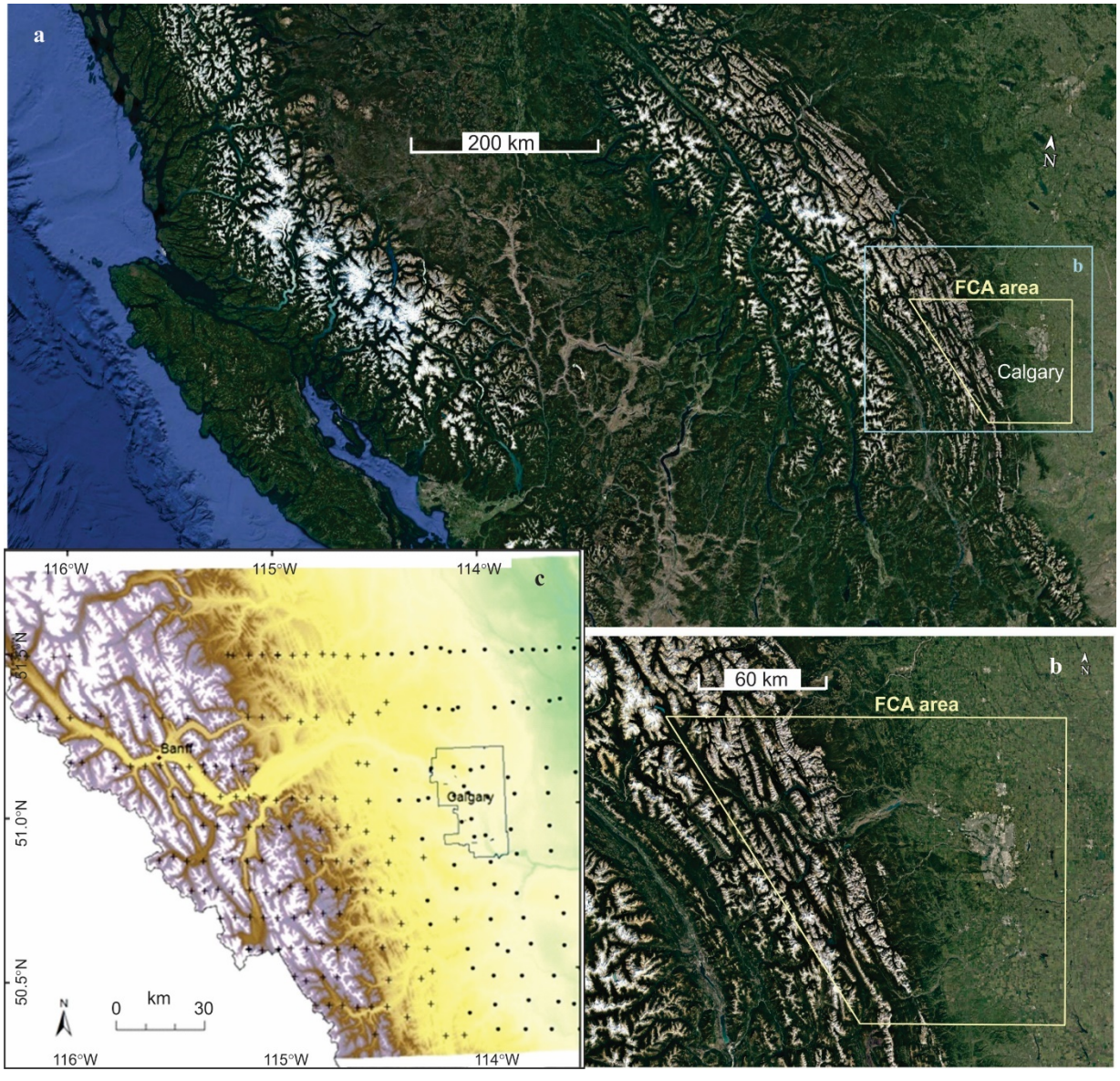

Figure 1. Foothills Climate Array (FCA) study region. (a) Location within southwestern Canada, with the blue inset indicating (b) the study setting within the regional context of the Canadian Rocky Mountains and the yellow inset indicating (c) the FCA site network. Images (a) and (b) are courtesy of Google Earth.

Earth Syst. Sci. Data Discuss., https://doi.org/10.5194/essd-2018-62
Manuscript under review for journal Earth Syst. Sci. Data
Discussion started: 4 June 2018

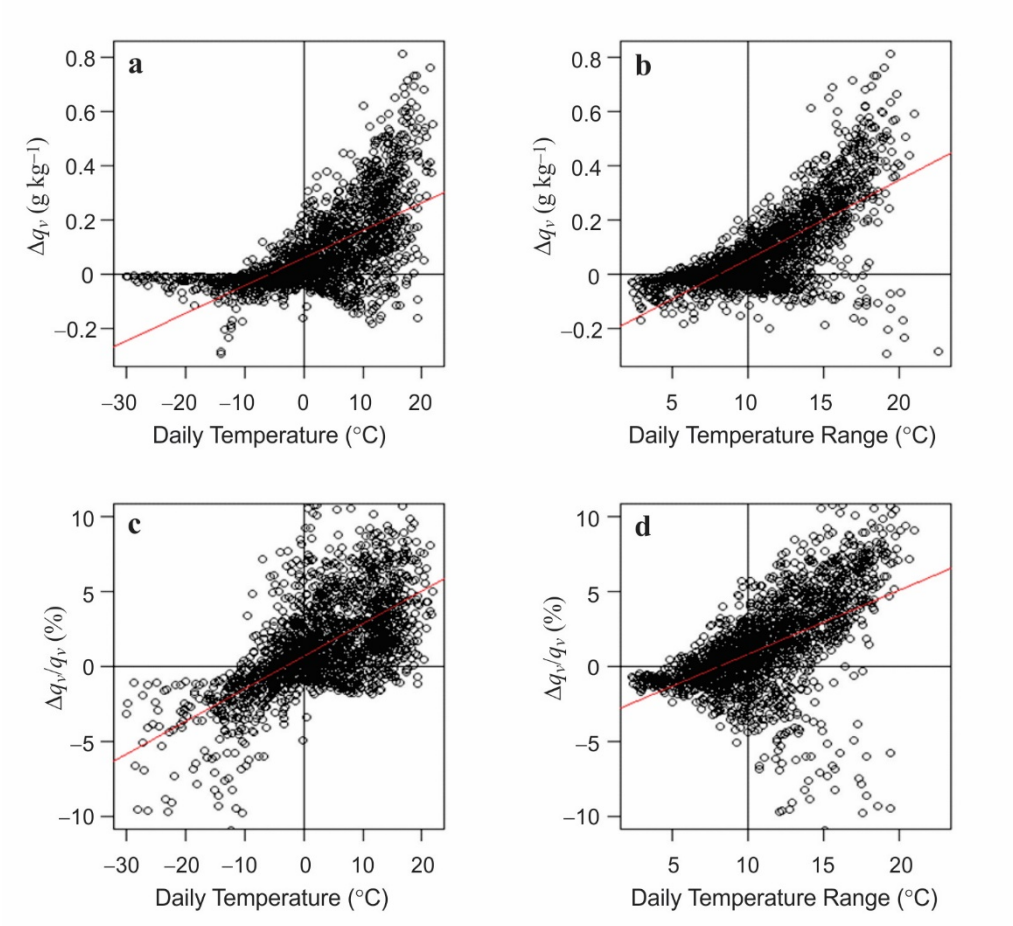

Figure 2. Difference in specific humidity calculated from daily mean *T* and *RH* (q_{vd}) and from hourly data (q_{vh}): $\Delta q_v = q_{vd} - q_{vh}$. Relation between Δq_v and (a, c) temperature and (b, d) daily temperature range. The top panels are actual differences, in g kg^{-1}, and the lower panels are normalized by mean daily q_v, expressed as the % difference.

Earth Syst. Sci. Data Discuss., https://doi.org/10.5194/essd-2018-62
Manuscript under review for journal Earth Syst. Sci. Data
Discussion started: 4 June 2018

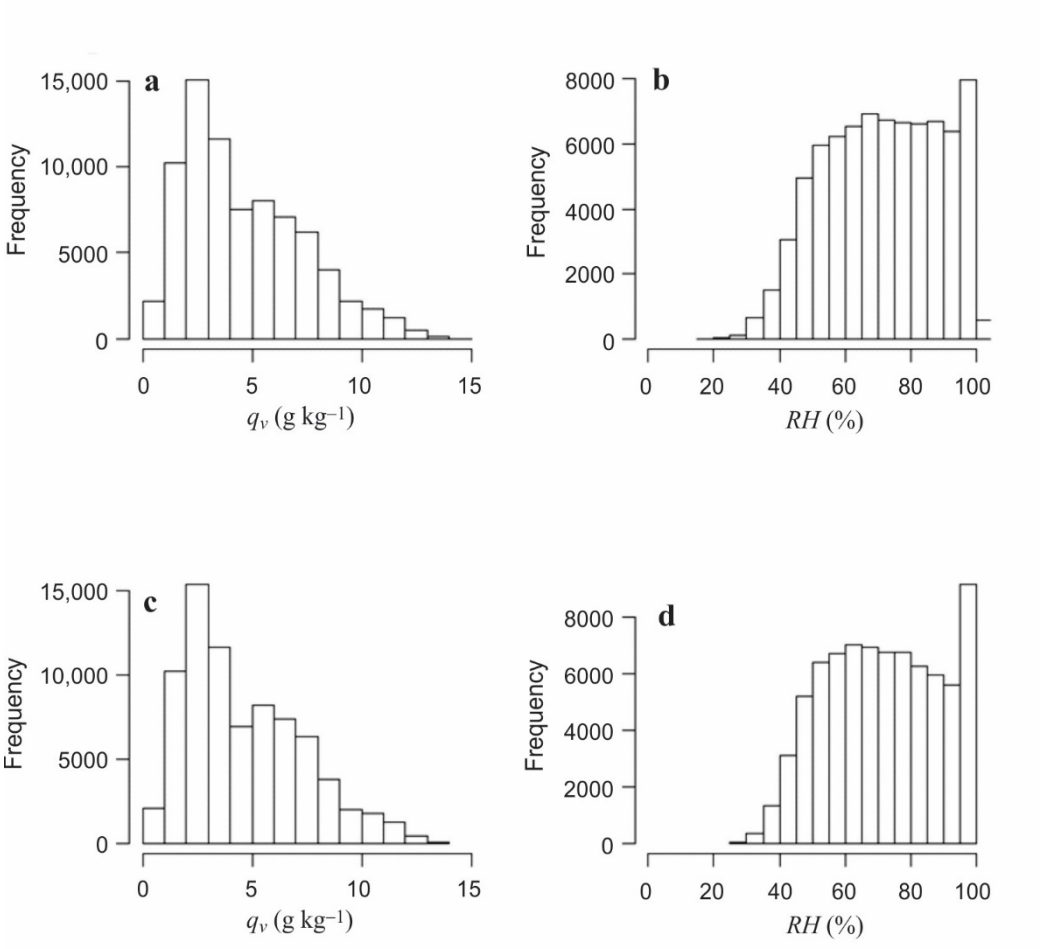

Figure 3. Frequency distributions of (a,b) actual and (c,d) interpolated specific and relative humidity, using the IDW model with the lowest interpolation errors. Specific humidity distributions are statistically equivalent, but the *RH* distributions differ.

Earth Syst. Sci. Data Discuss., https://doi.org/10.5194/essd-2018-62
Manuscript under review for journal Earth Syst. Sci. Data
Discussion started: 4 June 2018

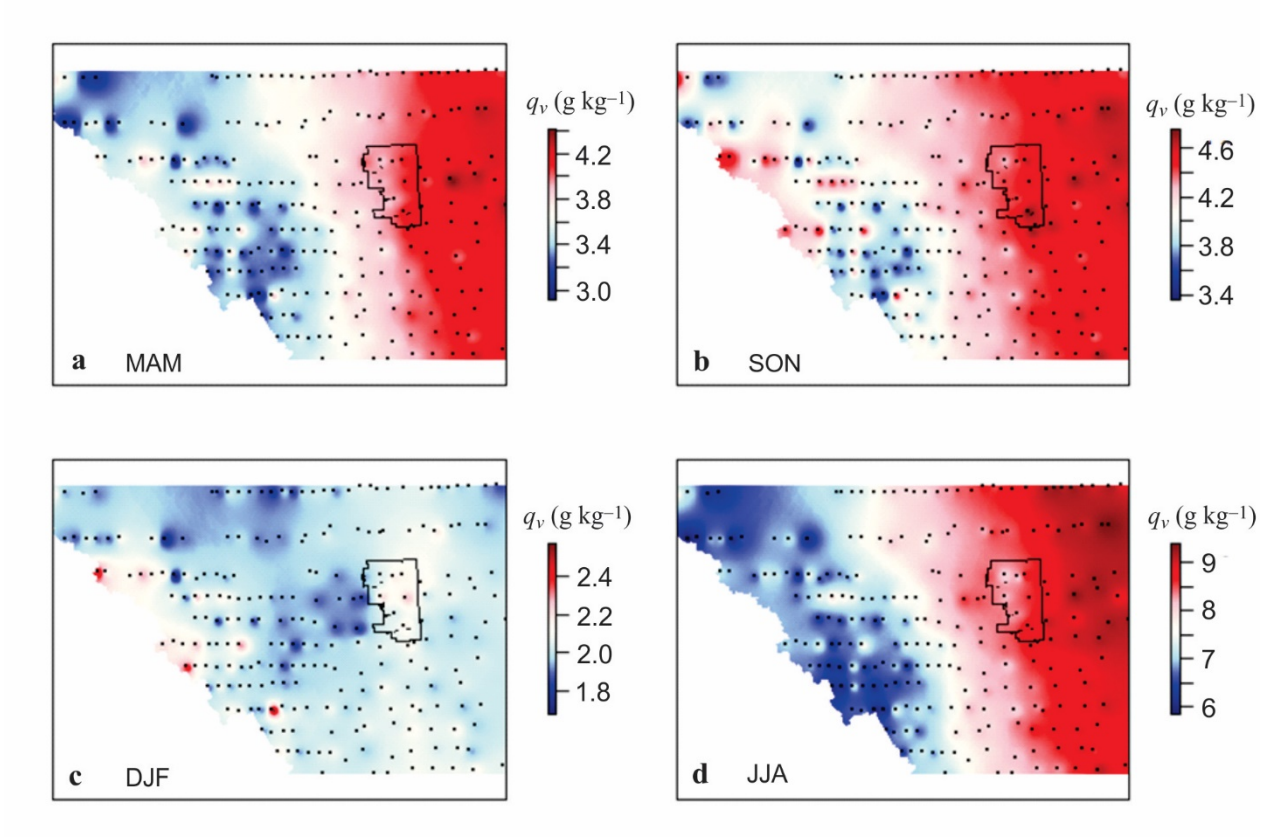

Figure 4. Mean seasonal values of specific humidity over the study region (g kg^{-1}): (a) spring (MAM), (b) autumn (SON), (c) winter (DJF) and (d) summer (JJA).

Earth Syst. Sci. Data Discuss., https://doi.org/10.5194/essd-2018-62
Manuscript under review for journal Earth Syst. Sci. Data
Discussion started: 4 June 2018

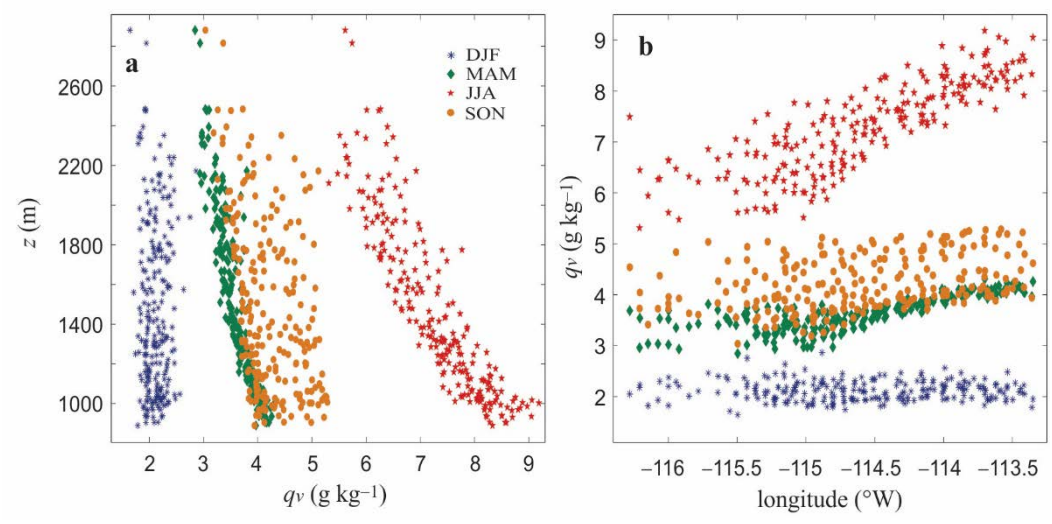

Figure 5. Mean seasonal specific humidity vs. (a) elevation and (b) longitude, for all sites. Values are a composite of five years in each seasonal record (i.e., average specific humidity at each site over 15 months). Winter (DJF) in blue, spring (MAM) in green, summer (JJA) in red, and autumn (SON) in orange.

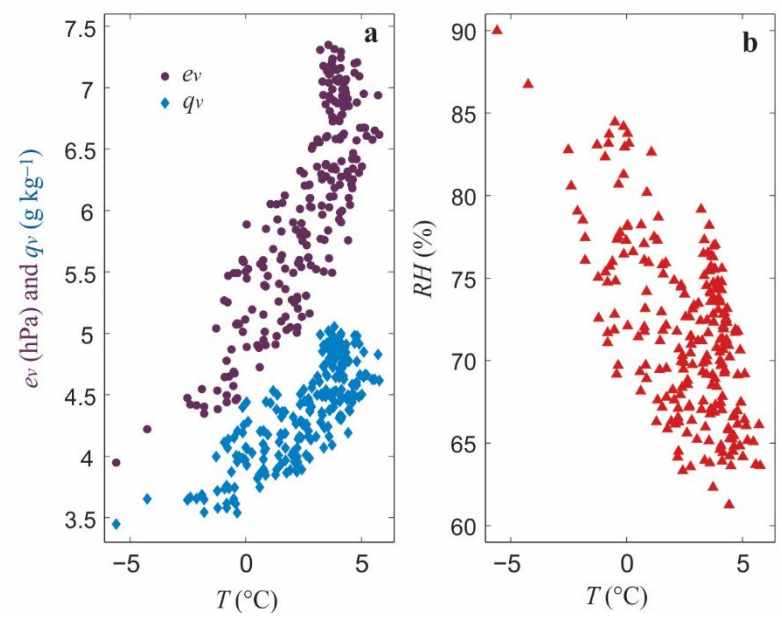

Figure 6. Mean annual humidity data as a function of mean annual temperature at each FCA site. (a) Vapour pressure (burgundy circles) and specific humidity (blue diamonds). (b) Relative humidity (red triangles).

Earth Syst. Sci. Data Discuss., https://doi.org/10.5194/essd-2018-62
Manuscript under review for journal Earth Syst. Sci. Data
Discussion started: 4 June 2018

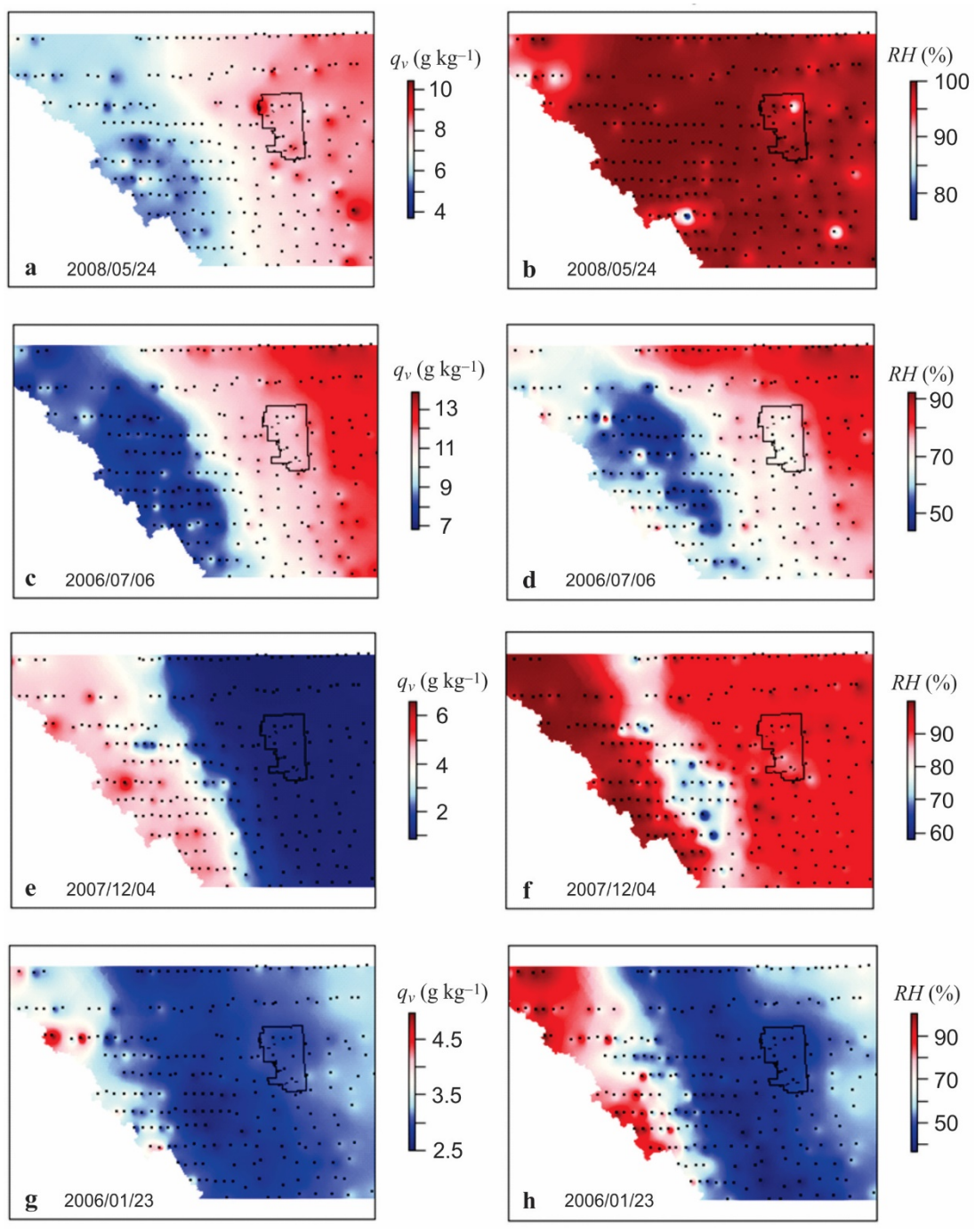

Figure 7. Examples of daily specific (left) and relative (right) humidity structure in the study area. (a, b) A cyclonic precipitation event on May 24, 2008. (c, d) A day with afternoon thunderstorm activity, July 6, 2006. (e, f) A continental polar air mass over the study area on December 4, 2007. (g, h) Chinook conditions on January 23, 2006.